
AGILEFORMER: SPATIALLY AGILE TRANSFORMER UNET FOR MEDICAL IMAGE SEGMENTATION

Peijie Qiu, Jin Yang

Mallinckrodt Institute of Radiology
Washington University School of Medicine
St. Louis, MO, USA
{peijie.qiu, jin.yang}@wustl.edu

Sayantana Kumar

Department of Computer Science and Engineering
Washington University in St. Louis
St. Louis, MO, USA

Soumyendu Sekhar Ghosh

Department of Electrical and Systems Engineering
Washington University in St. Louis
St. Louis, MO, USA

Aristeidis Sotiras

Mallinckrodt Institute of Radiology
Institute for Informatics, Data Science & Biostatistics
Washington University School of Medicine
St. Louis, MO, USA

ABSTRACT

In the past decades, deep neural networks, particularly convolutional neural networks, have achieved state-of-the-art performance in a variety of medical image segmentation tasks. Recently, the introduction of the vision transformer (ViT) has significantly altered the landscape of deep segmentation models. There has been a growing focus on ViTs, driven by their excellent performance and scalability. However, we argue that the current design of the vision transformer-based UNet (ViT-UNet) segmentation models may not effectively handle the heterogeneous appearance (e.g., varying shapes and sizes) of objects of interest in medical image segmentation tasks. To tackle this challenge, we present a structured approach to introduce spatially dynamic components to the ViT-UNet. This adaptation enables the model to effectively capture features of target objects with diverse appearances. This is achieved by three main components: **(i)** deformable patch embedding; **(ii)** spatially dynamic multi-head attention; **(iii)** deformable positional encoding. These components were integrated into a novel architecture, termed AgileFormer. AgileFormer is a spatially agile ViT-UNet designed for medical image segmentation. Experiments in three segmentation tasks using publicly available datasets demonstrated the effectiveness of the proposed method. The code is available at <https://github.com/sotiraslab/AgileFormer>.

Keywords Transformer · UNet · Medical Image Segmentation.

1 Introduction

Medical image segmentation tasks are important in modern medicine, as it is typically the first step in many image-driven diagnoses and analyses [1, 2]. Deep learning based automated segmentation methods have dominated this field due to their high efficiency and state-of-the-art performance. Among them, convolutional neural networks (CNNs) [3, 4, 5, 6, 7, 8] have emerged as the most prevalent choice since the introduction of UNet [3]. This is due to CNNs' inherent advantages in handling image-driven tasks, such as their ability to capture locality and translation invariance. However, they struggle with capturing global semantics primarily due to their restricted receptive field.

In contrast, the recently proposed vision transformer (ViT) [9] mitigates this problem through a self-attention mechanism that captures dependencies between image patches regardless of their spatial distances. The first ViT-based UNet (ViT-UNet) for medical image segmentation combined a ViT encoder with a CNN decoder, and hence was termed TransUNet [1]. However, TransUNet is burdened by a large number of parameters (~100M) and considerable computational complexity. This is because it employs standard self-attention, which has a quadratic time and memory

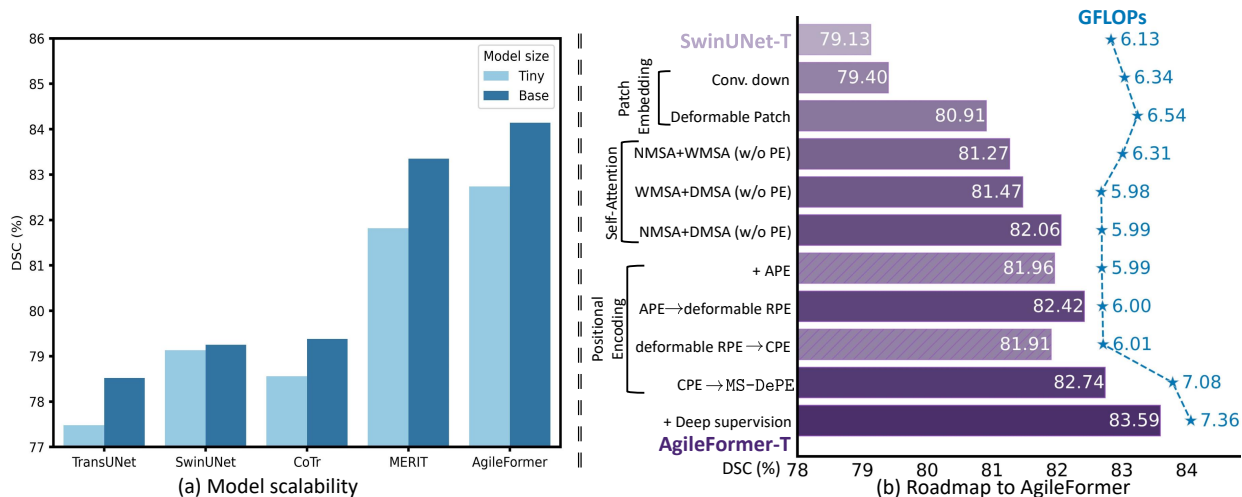


Figure 1: (a) Comparison of model scalability in the Synapse dataset. The base model is almost four times larger than the tiny model. (b) A roadmap going from SwinUNet to the proposed AgileFormer: from the top to the bottom, each row represents a model design variant. The foreground bars are DSC in the FLOP regime of different design variants; a hatched bar means the modification leads to a performance drop.

complexity w.r.t. the input token size. Leveraging the window attention [10], which performs self-attention within a small window in parallel for all image patches, SwinUNet [2] mitigates this challenge and is the first pure ViT-UNet, with self-attention as the main feature extractor. However, SwinUNet uses fixed-size windowing, which may limit its ability to capture precise representation for target objects with varying sizes and shapes. This potentially limits its adaptability and generalizability to multi-class segmentation tasks.

Additionally, SwinUNet do not exhibit good scaling behavior. In other words, their performance did not scale effectively when increasing the size of the model [2] (as evident in Fig. 1(a)). This is in contrast to evidence provided by empirical studies using natural images that have revealed that ViTs exhibit exceptional scaling behavior. We hypothesize this phenomenon may also be attributed to heterogeneity in the size and shape of objects targeted for segmentation, which cannot be handled by fixed-size windowing. To address these challenges, spatially dynamic components are necessary for improving the performance and scalability of a ViT-UNet. Although recent works have explored introducing dynamic (e.g., multi-scale [11], deformable [12, 13]) components into ViT-UNets for medical imaging, they have mainly focused on adopting existing deformable attention. However, they did not investigate introducing dynamic components into other parts (i.e., patch embedding and positional encoding) of a ViT-UNet. We argue that enhancing these other components with dynamic elements is equally important. We kindly direct the readers to Appendix A for an in-depth discussion on how AgileFormer fundamentally differs from the three aforementioned works [11, 12, 13].

Accordingly, we developed a novel spatially agile pure ViT-UNet to capture diverse target objects in a medical image segmentation task. First, we replace the standard rigid square patch embedding in ViT-UNet with a novel deformable patch embedding. Second, we adopt spatially dynamic self-attention [14] as the building block to capture spatially varying features. Third, we propose a novel multi-scale deformable positional encoding to model irregularly sampled grids in self-attention. We integrated these dynamic components into a novel ViT-UNet architecture, named **AgileFormer**. Extensive experiments demonstrated the effectiveness of the proposed method for three medical image segmentation tasks. AgileFormer outperformed recent state-of-the-art UNet models for medical image segmentation and demonstrated exceptional scalability.

2 Method

In this section, we provide a roadmap going from the standard SwinUNet to the proposed AgileFormer (see Fig. 1(b)). To make this paper self-contained, we first provide a brief introduction of the essential elements in ViT-UNets. A ViT-UNet (e.g., SwinUNet) is a U-shaped encoder-decoder network with skip connections, wherein the primary feature extractions in both the encoder and decoder are achieved by the self-attention mechanism. The building block of a standard ViT-UNet is composed of three fundamental components: patch embedding, self-attention, and positional encoding. The patch embedding projects image patches into feature embeddings. More recent ViTs [15, 14] even treat downsampling (i.e., patch merging in a SwinUNet) as part of the patch embedding. In this paper, we will follow

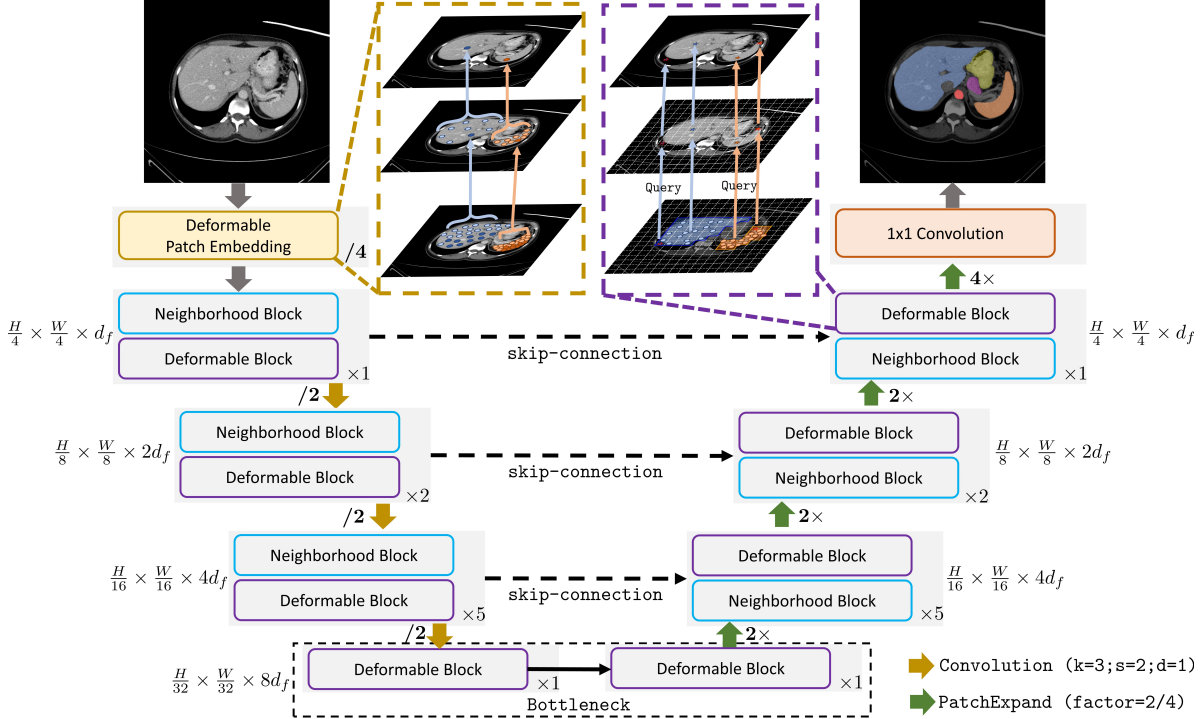


Figure 2: The architecture of the proposed AgileFormer.

the same convention. The self-attention, which captures the dependencies between image patches, is used for the main feature extraction. For computational tractability and the need of locality, recent ViT-UNets use window-based self-attention mechanism [2, 16, 13, 17]. Unlike convolution, self-attention discards the spatial correlation between image patches, which hinders the localization ability of pure ViT in segmentation task. The positional encoding is used to address this limitation. We would like to point out that there are also hybrid models [1, 16, 18, 17, 12, 19], where the main feature extraction in the encoder/decoder is achieved by both CNN and ViT. Whereas, we focus on developing a pure ViT-UNet in this paper.

The rest of this section is organized to introduce the three main components of the proposed AgileFormer in Fig. 2: deformable patch embedding (Section 2.1), spatially dynamic multi-head attention (Section 2.2), and deformable positional encoding (Section 2.3).

2.1 Deformable Patch Embedding

2.1.1 Rigid patch embedding

The ViT-UNet starts by converting image patches into tokens. This process typically involves partitioning an image into a sequence of non-overlapping $n \times n$ ($\times n$) (e.g., 4×4 ($\times 4$) in SwinUNet [2, 20, 17]) fixed-size patches. Subsequently, each of these patches is projected into a 1D feature vector. The main reason for performing a rigid (square) patch embedding is due to its simplicity, as it can be easily implemented as a standard convolution (kernel size $k = n$; stride $s = n$; dilation $d = 1$). However, we argue that this rigid patch embedding is not optimal for a segmentation task for two main reasons. First, segmentation requires more precise pixel-level localization. However, the rigid patch embedding can only provide patch-level localization. Second, the shape and size of target objects in most medical image segmentation tasks (e.g., the multi-organ segmentation task) vary significantly.

2.1.2 Deformable patch embedding

To address the limitation of rigid patch embedding, we propose a deformable patch embedding (see Fig. 2) by leveraging the deformable convolution [21]. The deformable convolution is defined as

$$(\mathbf{f} * \mathbf{k})[p] = \sum_{p_k \in \Omega} \phi(\mathbf{f}; p + \Delta p + p_k) \cdot \mathbf{k}[p_k], \quad (1)$$

where $\mathbf{f} \in \mathbb{R}^{L \times d_f}$ is a d_f -dimensional feature map with a uniform grid of L locations $p \in \mathbb{R}^{L \times D}$ ($D = 2$ for 2D; $D = 3$ for 3D). \mathbf{k} is the convolutional kernel that operates on the grid $\Omega = [p_k]$ defines k -nearest (i.e., kernel size) neighboring locations of p . $[\Delta p]$ are offsets from which the irregular grid is sampled. The offsets are learned through a single convolutional layer $\Delta p = \text{Conv}_{\text{offset}}(\mathbf{f})$. ϕ is a sampling function that performs bilinear/trilinear interpolation to sample locations $[p + \Delta p + p_k]$ in \mathbf{f} , as the offsets Δp are typically fractional.

First patch embedding. We replaced the single-layer rigid convolution patch embedding in a standard SwinUNet with two consecutive deformable convolutional layers ($k = 3$; $s = n/2$; $d = 1$). The rationale behind this is that the two consecutive overlapping deformable patch embeddings can extract better local representations, which compensates for the lack of locality in the self-attention.

Downsampling patch embedding. We also replaced the patch merging in standard SwinUNet with convolutional downsampling via a single layer ($k = 3$; $s = 2$; $d = 1$) for downsampling. We used overlapping kernels to better preserve localized patterns [22, 15, 20], which also aligns with the overlapping deformable patch embedding.

2.2 Spatially Dynamic Self-Attention

The self-attention is the building block of a ViT UNet. Unlike convolution, self-attention does not enforce any spatial inductive bias but makes decisions purely by relying on dependencies (mainly similarities) between tokens while lacking the ability to capture spatially adaptive features for multi-class segmentation. Accordingly, we propose using a spatially dynamic self-attention module as the building block of ViT-UNet. This module is inspired from [15], and it includes deformable multi-head attention (DMSA) [15] and neighborhood multi-head attention (NMSA) [23]. The transformer block is constructed by alternating these two attention mechanisms (see Fig. 2). We also distribute more computation to the third encoder block with a stage ratio of $[1 : 2 : 5 : 1]$, instead of $[2 : 2 : 2 : 2]$ in SwinUNet. This is because the third layer of the encoder typically captures better feature representations than the others [24].

2.2.1 Deformable Multi-head Self-Attention (DMSA)

The deformable multi-head (i.e., H head) attention [15] for the h -th head is formulated as

$$\text{DMSA}_h(\mathbf{f}) = \text{softmax}(\mathbf{Q}_h \tilde{\mathbf{K}}_h^\top / \sqrt{d_k}) \tilde{\mathbf{V}}_h \quad (2)$$

where:

$$\mathbf{Q}_h = \mathbf{f} \mathbf{W}_h^Q, \quad \tilde{\mathbf{K}}_h = \tilde{\mathbf{f}} \mathbf{W}_h^K, \quad \tilde{\mathbf{V}}_h = \tilde{\mathbf{f}} \mathbf{W}_h^V, \quad \tilde{\mathbf{f}} = \phi(\mathbf{f}; p + \Delta p_h). \quad (3)$$

Here, we reuse the notation in Eq. (1) with p being a uniform grid of points, Δp_h being the generated offsets for the h -th head, and ϕ being an interpolation function. $\{\mathbf{W}_h^Q, \mathbf{W}_h^K\} \in \mathbb{R}^{d_f \times d_k}$ and $\mathbf{W}_h^V \in \mathbb{R}^{d_f \times d_v}$ are trainable parameters, and d_k, d_v are the hidden dimensions of linear projection of the key $\tilde{\mathbf{K}}_h$ and the value $\tilde{\mathbf{V}}_h$ in DMSA. The offsets in DMSA are also generated by passing the query through a convolutional layer $\Delta p = \text{Conv}_{\text{offset}}(\mathbf{Q}_h)$. The resulting irregularly sampled feature map is denoted as $\tilde{\mathbf{f}}$ in Eq. (3). Similar to deformable convolution, the irregularly sampled feature map is then applied to self-attention by using irregularly sampled key $\tilde{\mathbf{K}}_h$ and value $\tilde{\mathbf{V}}_h$ (see Eq. (2)).

2.2.2 Neighborhood Multi-head Self-Attention (NMSA)

In contrast to standard self-attention, which computes the similarity of each element at a given position p on a feature map \mathbf{f} with every other element, the construction of neighborhood attention [23] only leverages the information from the k -nearest neighbors around location p . We reuse the notation k in Eq. (2), as the NMSA operates like a convolution. As a result, neighborhood attention reduces the quadratic computational complexity in standard self-attention to approximately linear w.r.t. the spatial dimension of \mathbf{f} , as k is typically small (e.g., $k = 7 \times 7$ ($\times 7$)). Furthermore, this reintroduces local operations into self-attention, allowing for translational equivariance, and thereby enhancing the ability to better preserve local information. Following the notation in Eq. (2), the neighborhood multi-head attention at position p_l is computed as

$$\text{NMSA}_h(\mathbf{f}[p_l]) = \text{softmax}(\mathbf{Q}_h[p_l] \hat{\mathbf{K}}_h[p_l]^\top / \sqrt{d_k}) \hat{\mathbf{V}}_h[p_l] \quad (4)$$

where:

$$\begin{aligned} \hat{\mathbf{K}}_h[p_l] &= [\mathbf{K}_h[p_{l1}], \dots, \mathbf{K}_h[p_{lk}]], & \mathbf{K}_h &= \mathbf{f} \mathbf{W}_h^K \\ \hat{\mathbf{V}}_h[p_l] &= [\mathbf{V}_h[p_{l1}]^\top, \dots, \mathbf{V}_h[p_{lk}]^\top]^\top, & \mathbf{V}_h &= \mathbf{f} \mathbf{W}_h^V. \end{aligned} \quad (5)$$

Here, $[p_{lk}]$ denotes the k -th neighboring locations for a given location p_l . It is worth noting that the dimension of the resulting attention is $\mathbb{R}^{L \times K}$ with $K = k \times k$ ($\times k$), instead of $\mathbb{R}^{L \times L}$ in standard self-attention or window-attention.

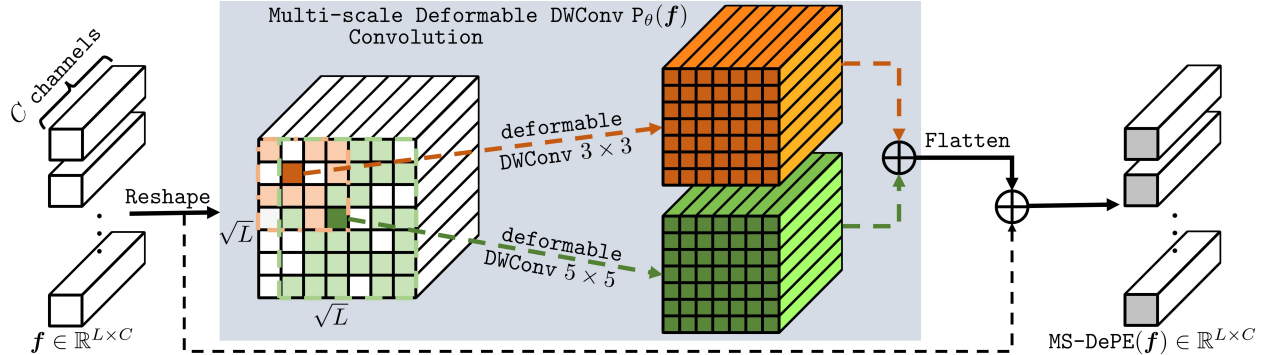


Figure 3: The proposed multi-scale deformable positional encoding for irregularly sampled grids in deformable multi-head self-attention.

2.3 Multi-scale Deformable Positional Encoding

The design of positional encoding (PE) is barely explored by previous ViT UNets. Most ViT-UNets either disregard positional encoding [1] or inherit PEs from their ancestor models [25, 2, 16]. Specifically, [25] used an absolute PE (APE), which assigns an absolute value for each token. While the others [2, 16, 20] used a relative PE (RPE) [26] to encode the relative positions between tokens. However, these are designed for 1D signals while neglecting the spatial correlation. Consequently, they are not well adapted for modeling 2D/3D signals with spatial correlations. Recently, conditional PE (CPE) [27] was designed for vision tasks offering the ability of both APE and RPE at the same time. More importantly, standard APE, RPE, and CPE are not directly applicable to irregularly sampled grids, as all of them are formulated in a rigid grid. In accordance with the irregularly sampled DMSA presented in this paper, we proposed a multi-scale deformable positional encoding (MS-DePE) designed to encode irregularly sampled positional information across various scales (see Fig. 3).

The proposed MS-DePE is formulated in a conditional positional encoding fashion [27] as follows:

$$\text{MS-DePE}(\mathbf{f}) = \mathbf{f} + \text{P}_\theta(\mathbf{f}), \quad (6)$$

where \mathbf{f} is the input feature map, and P_θ denotes the trainable positional encoding layer parameterized by θ . P_θ is implemented as multi-scale deformable depth-wise convolutional layers with different kernel sizes (i.e., 3×3 ($\times 3$) and 5×5 ($\times 5$)). For this purpose, we first recover the spatial resolution of the feature map \mathbf{f} before passing it through P_θ . After applying P_θ , we flatten the feature map back to its original shape (see Fig. 3 for details).

2.4 Model construction

Similar to [1, 2, 11], we developed two variants of AgileFormer by varying the embedding dimension (d_f) and the number of heads (H), but kept the main structures unchanged (i.e., number of transformer blocks in the encoder/decoder): AgileFormer-T(iny) ($d_f = [64, 128, 256, 512]$; $H = [2, 4, 8, 16]$) and AgileFormer-B(ase) ($d_f = [128, 256, 512, 1024]$; $H = [4, 8, 16, 32]$). We also incorporated deep supervision (DS) outlined in [7, 20] into the proposed method.

3 Experiments and results

3.1 Experimental design

Dataset. In line with previous works [1, 2, 20], we validated the effectiveness of the proposed method on three publicly available medical image segmentation datasets: the Synapse dataset [28], the Automated Cardiac Diagnosis Challenge (ACDC) dataset [29], and the brain tumor segmentation dataset from the Decathlon challenge [30]. The Synapse multi-organ dataset includes 30 3D abdominal CT scans with corresponding segmentation masks of 8 organs (i.e., aorta, gallbladder, kidney left, kidney right, liver, pancreas, spleen, stomach). The ACDC dataset consists of 100 3D cardiac MRI scans, each with a segmentation mask that features the right ventricle (RV), myocardium (Myo), and left ventricle (LV). The Decathlon brain tumor dataset comprises 484 3D multi-modal brain tumor MRI scans with segmentation masks delineating enhancing tumor, non-enhancing tumor, and edema. To be consistent with previous works [18, 20], we reported the results of the whole tumor (WT), enhancing tumor (ET) and tumor core (TC).

Experimental setup and evaluation metric. We adhered to the experimental protocols outlined in [1, 2] for the Synapse and ACDC datasets, including training/testing sets, input image size (i.e., 224×224), data augmentations,

Table 1: Performance comparison with 2D methods in the multi-organ segmentation using the Synapse dataset. The best result within each column is highlighted by **bold**, and the second-best is highlighted with an underline. †: models implemented by us. The other benchmarks were taken from [1, 2, 11, 19, 16, 31, 32, 33]. (*: $p < 0.01$; with the paired t-test to the second-best model. ∇: Large models that have a similar parameters to the AgileFormer-B model (TransCASCADE: 123.47M; MERIT: 147.86M; AgileFormer-B: 112.97M), where deep supervision is also applied.)

Methods		Avg DSC [†]	Aorta	Gallbladder	Kidney(L)	Kidney(R)	Liver	Pancreas	Spleen	Stomach
CNN	U-Net [3]	76.85	89.07	69.72	77.77	68.60	93.43	53.98	86.67	75.58
	R50 Att-UNet [1]	75.57	55.92	63.91	79.20	72.71	93.56	49.37	87.19	74.95
	Att-UNet [4]	77.77	89.55	68.88	77.98	71.11	93.57	58.04	87.30	75.75
Hybrid	TransUNet [1]	77.48	87.23	63.13	81.87	77.02	94.08	55.86	85.08	75.62
	MixedUNet [19]	78.59	87.92	64.99	81.47	77.29	93.06	59.46	87.75	76.81
	†CoTr [12]	78.56	87.09	65.37	86.19	80.32	94.22	52.28	87.01	76.00
	Hiformer [16]	80.29	85.63	73.29	82.39	64.84	94.22	60.84	91.03	78.07
	∇TransCASCADE [33]	82.68	86.63	68.48	87.66	84.56	94.43	65.33	90.79	83.69
ViT	R50 ViT [1]	71.29	73.73	55.13	75.80	72.20	91.51	45.99	81.99	73.95
	SwinUNet [2]	79.13	85.47	66.53	83.28	79.61	94.29	56.58	90.66	76.60
	TransDeepLab [34]	80.16	86.04	69.16	84.08	79.88	93.53	61.19	89.00	78.40
	†SDAUT [13]	80.67	87.03	69.30	81.87	80.20	94.91	64.56	89.54	77.91
	CATFormer [35]	82.17	88.98	67.16	85.72	81.69	95.34	66.53	90.74	81.20
	MissFormer [31]	81.96	86.99	68.65	85.21	82.00	94.41	65.67	91.92	80.81
	∇MERIT [11]	84.90	87.71	74.40	87.79	84.85	95.26	71.81	92.01	85.38
	†MERIT	82.89	87.42	72.61	87.94	85.36	94.45	67.63	87.15	80.53
	AgileFormer-T w/o DS	82.74	88.08	<u>75.16</u>	82.41	81.36	95.09	67.23	90.94	81.61
	AgileFormer-T w/ DS	83.59	88.81	74.43	84.61	82.78	<u>95.48</u>	69.45	90.14	83.05
AgileFormer-B w/o DS	84.14	87.76	74.71	86.69	83.81	95.31	68.28	91.00	85.58	
AgileFormer-B w/ DS	85.74*	<u>89.11</u>	77.89	88.83	85.00	95.64	<u>71.62</u>	92.20	85.63	
AgileFormer-B w/ DS [best]	86.11	89.29	78.51	89.09	85.12	95.96	71.52	93.03	86.35	

Note: MERIT uses the testing set to select the best model, which is not fair for comparison. The evaluation of MERIT using the last-epoch checkpoint results in a lower performance. AgileFormer can even achieve higher performance when using the testing set for model selection. We report this result as **AgileFormer-B w/s DS [best]** only for comparison, but we highly **discourage** any reader from citing this result.

Table 2: Performance comparison with 2D methods in cardiac MRI segmentation using the ACDC dataset. †: models implemented by us. The other benchmarks were taken from [1, 2, 19, 31, 33, 11].

Methods	Avg DSC [†]	RV	Myo	LV
TransUNet [1]	89.71	88.86	84.53	95.73
†CoTr [12]	90.52	87.81	88.44	95.29
SwinUNet [2]	90.00	88.55	85.62	95.83
MixedUNet [19]	90.43	86.64	89.04	95.62
MissFormer [31]	90.86	89.55	88.04	94.99
†SDAUT [13]	91.08	89.37	88.58	95.28
∇PVT-CASCADDE [33]	91.46	88.00	89.97	95.50
∇TransCASCADE [33]	91.63	89.14	90.25	95.50
∇MERIT [11]	<u>92.32</u>	<u>90.87</u>	<u>90.00</u>	<u>96.08</u>
AgileFormer-T w/ DS	91.76	89.80	89.71	95.77
AgileFormer-B w/ DS	92.55*	91.05	90.40	96.19

Table 3: Performance comparison with 3D models in brain tumor segmentation using the Decathlon dataset. †: models implemented by us. The input size was set to $96 \times 96 \times 96$. Please refer to Appendix A for details of implementing the 3D experiments. We only compared the tiny model (AgileFormer-T), as it has a similar scale to the baselines.

Methods	Avg DSC [†]	WT	ET	TC
†TransUNet [1]	84.6	90.5	79.9	83.4
†TransBTS [25]	84.2	90.2	<u>79.6</u>	82.9
†CoTr [12]	84.1	<u>91.2</u>	78.7	83.2
†UNETR [18]	84.1	90.5	79.3	82.4
†SwinUNETR [17]	<u>84.9</u>	90.7	80.5	83.5
†nnFormer [20]	<u>84.9</u>	91.4	79.2	<u>84.0</u>
AgileFormer-T w/ DS	85.7*	<u>91.2</u>	80.8	85.1

model selection, and evaluations. For a fair comparison with the previous literature, experiments for Synapse and ACDC datasets were carried out in 2D. For the 3D volumetric brain tumor segmentation, we followed the experimental protocols specified in [18] for a fair comparison with the previous literature. The input image was set to $96 \times 96 \times 96$. We evaluated the segmentation performance using the dice similarity coefficient (DSC). Statistical significance between the average DSC of the best and second-best model was estimated using the paired t-test. We emphasize that all competing methods applied in the Synapse, ACDC, and Decathlon datasets followed the same experimental protocols.

Implementation details. All models were trained using a combination of dice and cross-entropy loss [2, 20], employing an AdamW [36] optimizer with cosine learning rate decay and a 20-epoch warmup. We initialized model parameters with ImageNet pre-trained weights. In the 2D experiments, a batch size of 24 was used, the initial learning rate was set to 3×10^{-4} , and the model was trained for 400 epochs. For the 3D experiments, the batch size and learning rate were set to 4 and 5×10^{-4} , and the model was trained for 200 epochs. We would like to point out that we reimplemented all the 3D baseline models using the nnFormer framework (see Appendix B for details of 3D experiments). All experiments were implemented using PyTorch and were performed on a Nvidia V100 GPU with 32GB memory.

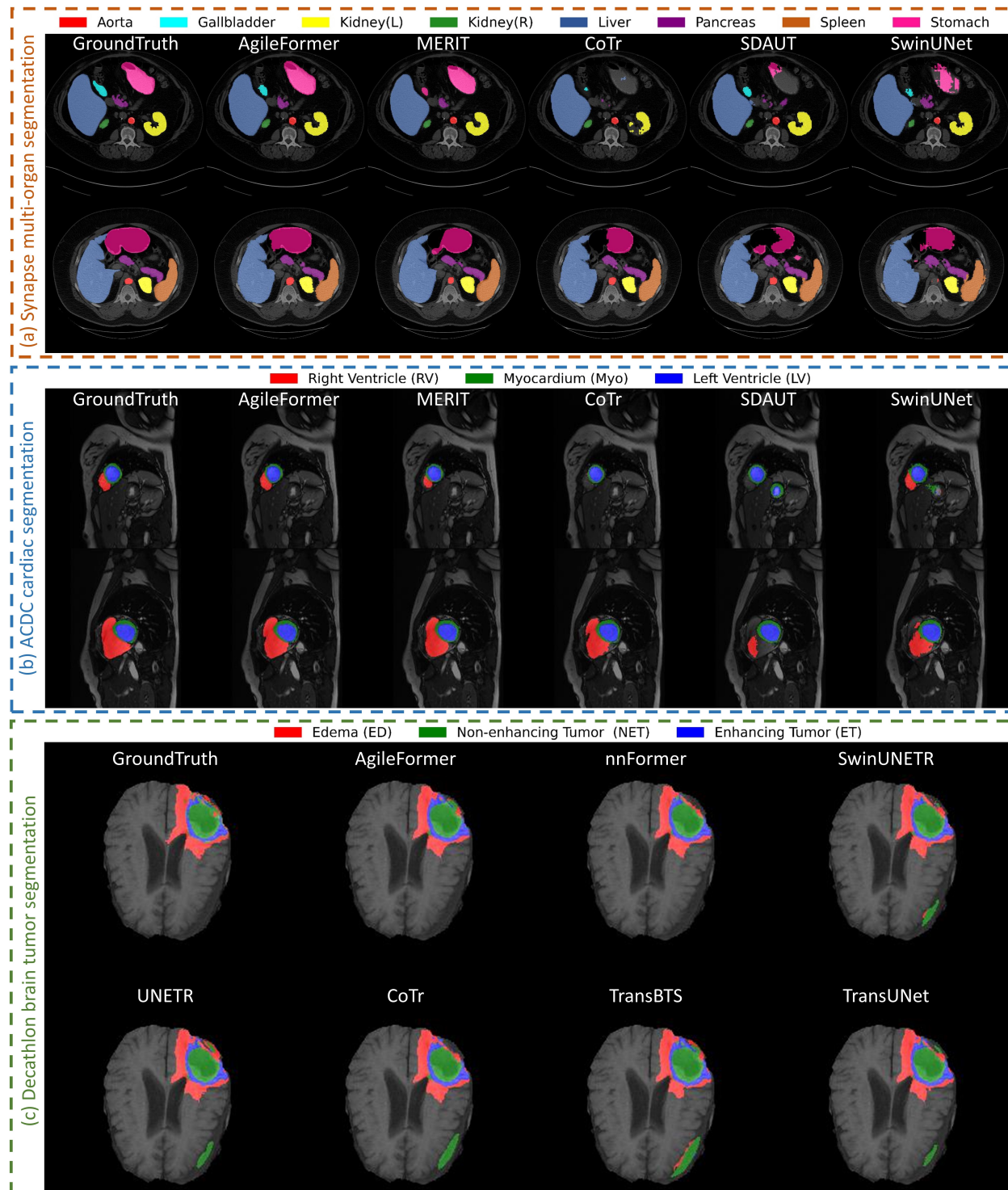


Figure 4: Visual comparison of (a) multi-organ, (b) cardiac, and (c) brain tumor segmentation across Synapse, ACDC, and Decathlon datasets. AgileFormer shows the best qualitative segmentation quality across all three datasets.

3.2 Main results

Our proposed AgileFormer outperformed recent state-of-the-art (SOTA) methods in all three datasets (Table 1, 2 and 3). Specifically, the proposed method performed better than the second-best model by 0.84, 0.23, and 0.80 in average DSC

Table 4: Ablation studies on model design variants in Synapse multi-organ segmentation task, starting from a SwinUNet baseline. This is also the roadmap going from SwinUNet to the proposed AgileFormer.

	Avg DSC \uparrow	Aorta	Gallbladder	Kidney(L)	Kidney(R)	Liver	Pancreas	Spleen	Stomach	Parms (M) /FLOPs (G)
Baseline (WMSA + RPE)	79.13	85.47	66.53	83.28	79.61	94.29	56.58	90.66	76.60	27.17 / 6.13
Convolutional Downsampling	79.40	85.74	70.56	82.33	80.69	93.50	58.89	91.46	72.05	29.10 / 6.34
Deformable Patch Embedding	80.91	87.38	71.25	85.17	83.08	94.11	58.71	88.92	78.67	29.14 / 6.54
NMSA + WMSA (w/o PE)	81.27	87.22	68.79	84.73	79.49	95.31	63.13	90.62	80.86	26.74 / 6.31
WMSA + DMSA (w/o PE)	81.47	86.12	67.37	84.18	80.13	95.61	64.86	90.97	82.55	26.77 / 5.98
NMSA + DMSA (w/o PE)	82.06	87.54	70.95	81.90	79.29	95.36	68.03	90.72	82.72	26.82 / 5.99
+ APE	81.96	88.35	70.72	81.82	78.84	95.09	67.80	90.27	82.45	28.90 / 5.99
APE \rightarrow deformable RPE [15]	82.42	87.17	73.32	86.08	82.54	95.08	65.65	88.64	80.92	26.99 / 6.00
deformable RPE \rightarrow CPE	81.91	88.13	72.28	79.81	77.75	95.06	65.24	91.90	85.14	26.87 / 6.01
CPE \rightarrow MS-DePE	82.74	88.08	75.16	82.41	81.36	95.09	67.23	90.94	81.61	27.47 / 7.08
+ Deep Supervision	83.59	88.81	74.43	84.61	82.78	95.48	69.45	90.14	83.05	28.85 / 7.36

(%) for Synapse multi-organ, ACDC cardiac, and brain tumor segmentation tasks, respectively. This improvement was shown to be statistically significant. Specifically, the proposed method achieved an average DSC of 85.74, surpassing the other baseline methods in segmenting all 6 out of 8 organs in the Synapse dataset (Table 1). For the remaining two organs, the proposed method is the second-best performing method. The proposed method achieved an average DSC of 92.55 in the ACDC dataset, surpassing all the baseline methods in segmenting RV, Myo, and LV (see Table 2). In the 3D volumetric brain tumor segmentation task, the proposed method achieved an average DSC of 85.7, surpassing recent SOTA ViT-UNet methods (Table 3). In addition, the proposed method demonstrated the best qualitative segmentation quality across these three public datasets (see Fig. 4).

3.3 Ablations on model design variants

We conducted ablation studies on the model design variants, including patch embedding and different choices of spatially dynamic attention and positional encoding (see Table 4). First, we showed that replacing patch merging with convolutional downsampling led to a small performance gain of 0.34% in average DSC. Then, adding deformable embedding can lead to a performance gain of 1.9% in DSC. Second, we ablated different choices of spatially dynamic self-attention by alternating window/ deformable/neighborhood attention. We removed positional encoding to eliminate its effect for now. Alternating window attention (WMSA) with both DMSA and NSMA led to a performance gain of 0.7% (DMSA) and 0.4% (NSMA), respectively. Alternating NMSA and DMSA resulted in a performance gain of 1.4%. Third, we brought back positional encoding, demonstrating that not all PEs can lead to a performance gain, e.g., adding APE and CPE even led to a performance drop. This is because these two PEs were not designed for irregularly sampled grids introduced by DMSA. Instead, the proposed MS-DePE improved performance by 0.8%. Notably, the proposed AgileFormer did not lead to a huge computational burden, with only a 1.1% increase in the number of parameters and a 15% rise in floating point operations, compared to SwinUNet.

3.4 Model scaling behavior

We compared the model scaling behavior of the proposed method with other ViT-UNets. As shown in Fig. 1(a), the proposed method demonstrated improved performance with growing model sizes for the Synapse multi-organ segmentation task, where different organs exhibit a lot of variability in shape and size. Specifically, the performance was improved by 2.15 in DSC (%) going from AgileFormer-T to AgileFormer-B, with parameters increase of approximately fourfold from 28.85M to 123.47M. We also observed that the methods with dynamic modules scaled better than those without dynamic modules, except for CoTr and SDAUT. We hypothesized this might be attributed to the fact that the main backbone of CoTr was still a CNN. Besides, deformable modules in both CoTr and SDAUT were only placed in the bottleneck.

4 Conclusion

In this paper, we proposed AgileFormer that systematically introduced spatially dynamic components (i.e., deformable patch embedding, spatially dynamic self-attention, and multi-scale deformable positional encoding) into a UNet for capturing spatially dynamic information for diverse target objects in the medical image segmentation. Extensive experiments demonstrated the effectiveness of the proposed method for a variety of medical image segmentation tasks. We aspire that the idea of systematically introducing spatially dynamic components to ViT-UNet will guide future designs on how to extract spatially dynamic representation for medical image segmentation with multiple targets.

Appendix

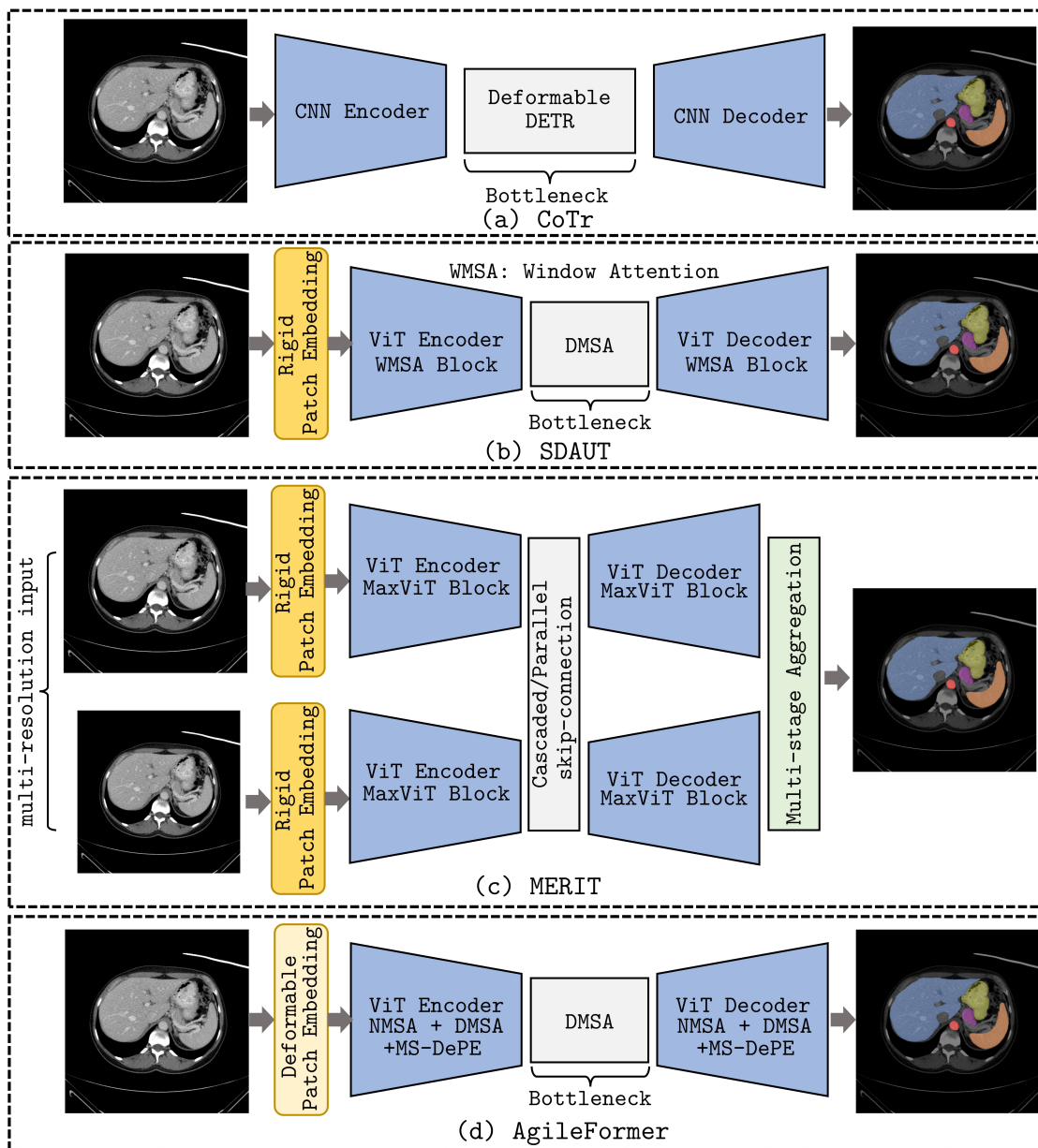


Figure 5: (a) CoTr is a hybrid model where Deformable DETR [37] was applied to the bottleneck. (b) SDAUT is a ViT-UNet originally proposed for medical image restoration. The encoder/decoder of SDAUT used window attention (WMSA); while DMSA was applied to the bottleneck. (c) MERIT captured dynamic feature representations using a multi-resolution and multi-stage approach, with the MaxViT [38] as the building block. (d) AgileFormer alternated NMSA and DMSA as the building block, adding novel deformable patch embedding and multi-scale deformable positional encoding.

A Comparison with other dynamic ViT-UNets

CoTr. Similar to its ancestor model [37], CoTr is a hybrid model where the main backbone (encoder/decoder) is still a CNN. Multi-scale deformable attention outlined in [37] serves as a bottleneck. As a result, it can only introduce limited deformability to capture spatially dynamic feature representation, as the main feature extractor does not have spatially dynamic components. In addition, CoTr does not take full advantage of ViT to capture long-range dependencies as its

main backbone is still a CNN. We hypothesize these factors may limit its scalability (see evidence in Appendix C). **Instead**, the proposed method uses a ViT as the main backbone (encoder/decoder), where neighborhood attention and deformable attention [15] serve as the main building blocks, which better preserves the advantage of ViT while having the additional advantage of capturing spatially localized and dynamic features.

SDAUT. Although SDAUT also uses the deformable attention mechanism [15] as the proposed method, it is primarily proposed for image restoration tasks instead of a segmentation task. The optimal architecture of SDAUT uses a combination of window attention and deformable attention, where deformable attention is applied only to the third encoder and decoder. **Instead**, the deformable attention is applied at every layer (encoder/decoder) of the proposed method, which facilitates the extraction of spatially dynamic features. In addition, we further introduce deformable patch embedding to fundamentally change the rigid patch embedding. We also introduce a multi-scale deformable positional encoding to handle the irregularly sampled grid introduced by the deformable attention. We found that *those two novel components are as important as spatially dynamic attention* to enhance the segmentation performance.

MERIT. MERIT mainly takes advantage of multi-resolution information to capture spatially dynamic (mainly varying size) features, by combining the features extracted from inputs of different sizes. **Instead**, the proposed method handles both varying sizes as well as varying shapes by spatially dynamic attention. Whereas, we use a multi-scale deformable positional encoding to further capture multi-scale information.

B Implementation details on 3D experiments

We found that the comparison in nnFormer [20] was unfair. nnFormer and SwinUNETR take images with a size of $128 \times 128 \times 128$ as input; while the results reported by UNETR were achieved with inputs of a size of $96 \times 96 \times 96$ in our implementation. As a result, the input image size was set to $96 \times 96 \times 96$ for all methods. We also found that there was a huge performance gap between nnFormer and the other methods (i.e., TransUNet, TransBTS, UNETR, SwinUNETR, and CoTr), which is not consistent with the performance on other segmentation tasks. We conjectured that this performance gap might be attributed to different preprocessing, training, and evaluation procedures. Therefore, in our experiments, we retrained all the methods using the nnFormer codebase to standardize the comparison. For the proposed method, the batch size was set to 4, and the initial learning rate was set to 5×10^{-4} . For the baseline methods, we followed the default hyperparameter settings in their original papers. We **found** out that our reimplemention resulted in a higher performance of TransUNet, TransBTS, UNETR, SwinUNETR, and CoTr compared to results reported in nnFormer, even with a smaller size input.

We then discuss how the 3D deformable attention and neighborhood attention were implemented in the proposed method: **(i) 3D deformable multi-head attention** was implemented by our own in plain PyTorch. First, we replaced the 2D convolution with the 3D convolution to generate the offset points ($\text{Conv}_{\text{offset}}(\mathbf{Q}_h)$). Second, we sampled positions in the 3D grid based on the generated offset points. For this purpose, we use `torch.functional.grid_sample` (implemented in CUDA) to sample fractional offset positions. Third, for the key and query projection, we kept the 2D 1×1 convolutional projection. This is because the 2D and 3D convolution with a kernel size of 1 essentially performs the same weighted summation over channels. We first reshape the 5D tensor of size $[B \times C \times D \times H \times W]$ into a 4D tensor $[B \times C \times 1 \times (D * H * W)]$ and then perform a 2D 1×1 convolution. After finishing the computation of self-attention, we reshape the 4D tensor back to 5D to restore its spatial dimension. **(ii)** The official implementation¹ of **3D neighborhood multi-head attention** supports an efficient CUDA implementation. So we directly adopted their implementation without further change.

References

- [1] Jieneng Chen, Yongyi Lu, Qihang Yu, Xiangde Luo, Ehsan Adeli, Yan Wang, Le Lu, Alan L Yuille, and Yuyin Zhou. Transunet: Transformers make strong encoders for medical image segmentation. *arXiv preprint arXiv:2102.04306*, 2021.
- [2] Hu Cao, Yueyue Wang, Joy Chen, Dongsheng Jiang, Xiaopeng Zhang, Qi Tian, and Manning Wang. Swin-unet: Unet-like pure transformer for medical image segmentation. In *European conference on computer vision*, pages 205–218. Springer, 2022.
- [3] Olaf Ronneberger, Philipp Fischer, and Thomas Brox. U-net: Convolutional networks for biomedical image segmentation. In *MICCAI 2015: 18th International Conference, Munich, Germany, October 5-9, 2015, Proceedings, Part III 18*, pages 234–241. Springer, 2015.

¹<https://github.com/SHI-Labs/NATTEN>

- [4] Ozan Oktay, Jo Schlemper, Loic Le Folgoc, Matthew Lee, Mattias Heinrich, Kazunari Misawa, Kensaku Mori, Steven McDonagh, Nils Y Hammerla, Bernhard Kainz, et al. Attention u-net: Learning where to look for the pancreas. *arXiv preprint arXiv:1804.03999*, 2018.
- [5] Ho Hin Lee, Shunxing Bao, Yuankai Huo, and Bennett A Landman. 3d ux-net: A large kernel volumetric convnet modernizing hierarchical transformer for medical image segmentation. *arXiv preprint arXiv:2209.15076*, 2022.
- [6] Jin Yang, Daniel S Marcus, and Aristeidis Sotiras. Dynamic u-net: Adaptively calibrate features for abdominal multi-organ segmentation. *arXiv preprint arXiv:2403.07303*, 2024.
- [7] Fabian Isensee, Philipp Kickingereder, Wolfgang Wick, Martin Bendszus, and Klaus H Maier-Hein. Brain tumor segmentation and radiomics survival prediction: Contribution to the brats 2017 challenge. In *Brainlesion: Glioma, Multiple Sclerosis, Stroke and Traumatic Brain Injuries: Third International Workshop, BrainLes 2017, Held in Conjunction with MICCAI 2017, Quebec City, QC, Canada, September 14, 2017, Revised Selected Papers 3*, pages 287–297. Springer, 2018.
- [8] Fabian Isensee, Paul F Jaeger, Simon AA Kohl, Jens Petersen, and Klaus H Maier-Hein. nnu-net: a self-configuring method for deep learning-based biomedical image segmentation. *Nature methods*, 18(2):203–211, 2021.
- [9] Alexey Dosovitskiy, Lucas Beyer, Alexander Kolesnikov, Dirk Weissenborn, Xiaohua Zhai, Thomas Unterthiner, Mostafa Dehghani, Matthias Minderer, Georg Heigold, Sylvain Gelly, et al. An image is worth 16x16 words: Transformers for image recognition at scale. In *International Conference on Learning Representations*, 2020.
- [10] Ze Liu, Yutong Lin, Yue Cao, Han Hu, Yixuan Wei, Zheng Zhang, Stephen Lin, and Baining Guo. Swin transformer: Hierarchical vision transformer using shifted windows. In *Proceedings of the IEEE/CVF international conference on computer vision*, pages 10012–10022, 2021.
- [11] Md Mostafijur Rahman and Radu Marculescu. Multi-scale hierarchical vision transformer with cascaded attention decoding for medical image segmentation. In *Medical Imaging with Deep Learning*, pages 1526–1544. PMLR, 2024.
- [12] Yutong Xie, Jianpeng Zhang, Chunhua Shen, and Yong Xia. Cotr: Efficiently bridging cnn and transformer for 3d medical image segmentation. In *MICCAI 2021: 24th International Conference, Strasbourg, France, September 27–October 1, 2021, Proceedings, Part III 24*, pages 171–180. Springer, 2021.
- [13] Jiahao Huang, Xiaodan Xing, Zhifan Gao, and Guang Yang. Swin deformable attention u-net transformer (sdaut) for explainable fast mri. In *International Conference on Medical Image Computing and Computer-Assisted Intervention*, pages 538–548. Springer, 2022.
- [14] Zhuofan Xia, Xuran Pan, Shiji Song, Li Erran Li, and Gao Huang. Dat++: Spatially dynamic vision transformer with deformable attention. *arXiv preprint arXiv:2309.01430*, 2023.
- [15] Zhuofan Xia, Xuran Pan, Shiji Song, Li Erran Li, and Gao Huang. Vision transformer with deformable attention. In *Proceedings of the IEEE/CVF conference on computer vision and pattern recognition*, pages 4794–4803, 2022.
- [16] Moein Heidari, Amirhossein Kazerouni, Milad Soltany, Reza Azad, Ehsan Khodapanah Aghdam, Julien Cohen-Adad, and Dorit Merhof. Hiformer: Hierarchical multi-scale representations using transformers for medical image segmentation. In *Proceedings of the IEEE/CVF Winter Conference on Applications of Computer Vision*, pages 6202–6212, 2023.
- [17] Ali Hatamizadeh, Vishwesh Nath, Yucheng Tang, Dong Yang, Holger R Roth, and Daguang Xu. Swin unetr: Swin transformers for semantic segmentation of brain tumors in mri images. In *International MICCAI Brainlesion Workshop*, pages 272–284. Springer, 2021.
- [18] Ali Hatamizadeh, Yucheng Tang, Vishwesh Nath, Dong Yang, Andriy Myronenko, Bennett Landman, Holger R Roth, and Daguang Xu. Unetr: Transformers for 3d medical image segmentation. In *Proceedings of the IEEE/CVF winter conference on applications of computer vision*, pages 574–584, 2022.
- [19] Hongyi Wang, Shiao Xie, Lanfen Lin, Yutaro Iwamoto, Xian-Hua Han, Yen-Wei Chen, and Ruofeng Tong. Mixed transformer u-net for medical image segmentation. In *ICASSP*, pages 2390–2394. IEEE, 2022.
- [20] Hong-Yu Zhou, Jiansen Guo, Yinghao Zhang, Xiaoguang Han, Lequan Yu, Liansheng Wang, and Yizhou Yu. nnformer: Volumetric medical image segmentation via a 3d transformer. *IEEE Transactions on Image Processing*, 2023.
- [21] Jifeng Dai, Haozhi Qi, Yuwen Xiong, Yi Li, Guodong Zhang, Han Hu, and Yichen Wei. Deformable convolutional networks. In *Proceedings of the IEEE international conference on computer vision*, pages 764–773, 2017.
- [22] Huaibo Huang, Xiaoqiang Zhou, Jie Cao, Ran He, and Tieniu Tan. Vision transformer with super token sampling. In *Proceedings of the IEEE/CVF Conference on Computer Vision and Pattern Recognition*, pages 22690–22699, 2023.

- [23] Ali Hassani, Steven Walton, Jiachen Li, Shen Li, and Humphrey Shi. Neighborhood attention transformer. In *Proceedings of the IEEE/CVF Conference on Computer Vision and Pattern Recognition*, pages 6185–6194, 2023.
- [24] Haonan Wang, Peng Cao, Jiaqi Wang, and Osmar R Zaiane. Uctransnet: rethinking the skip connections in u-net from a channel-wise perspective with transformer. In *Proceedings of the AAAI conference on artificial intelligence*, volume 36, pages 2441–2449, 2022.
- [25] Wenxuan Wang, Chen Chen, Meng Ding, Hong Yu, Sen Zha, and Jiangyun Li. Transbts: Multimodal brain tumor segmentation using transformer. In *MICCAI 2021: 24th International Conference, Strasbourg, France, September 27–October 1, 2021, Proceedings, Part I 24*, pages 109–119. Springer, 2021.
- [26] Peter Shaw, Jakob Uszkoreit, and Ashish Vaswani. Self-attention with relative position representations. In *Proceedings of NAACL-HLT*, pages 464–468, 2018.
- [27] Xiangxiang Chu, Zhi Tian, Bo Zhang, Xinlong Wang, and Chunhua Shen. Conditional positional encodings for vision transformers. In *The Eleventh International Conference on Learning Representations*, 2022.
- [28] Bennett Landman, Zhoubing Xu, J Igelsias, Martin Styner, T Langerak, and Arno Klein. Miccai multi-atlas labeling beyond the cranial vault—workshop and challenge. In *Proc. MICCAI Multi-Atlas Labeling Beyond Cranial Vault—Workshop Challenge*, volume 5, page 12, 2015.
- [29] Olivier Bernard, Alain Lalonde, Clement Zotti, Frederick Cervenansky, Xin Yang, Pheng-Ann Heng, Irem Cetin, Karim Lekadir, Oscar Camara, Miguel Angel Gonzalez Ballester, et al. Deep learning techniques for automatic mri cardiac multi-structures segmentation and diagnosis: is the problem solved? *IEEE transactions on medical imaging*, 37(11):2514–2525, 2018.
- [30] Michela Antonelli, Annika Reinke, Spyridon Bakas, Keyvan Farahani, Annette Kopp-Schneider, Bennett A Landman, Geert Litjens, Bjoern Menze, Olaf Ronneberger, Ronald M Summers, et al. The medical segmentation decathlon. *Nature communications*, 13(1):4128, 2022.
- [31] Xiaohong Huang, Zhifang Deng, Dandan Li, Xueguang Yuan, and Ying Fu. Missformer: An effective transformer for 2d medical image segmentation. *IEEE Transactions on Medical Imaging*, 2022.
- [32] Xiangyi Yan, Hao Tang, Shanlin Sun, Haoyu Ma, Deying Kong, and Xiaohui Xie. After-unet: Axial fusion transformer unet for medical image segmentation. In *Proceedings of the IEEE/CVF winter conference on applications of computer vision*, pages 3971–3981, 2022.
- [33] Md Mostafijur Rahman and Radu Marculescu. Medical image segmentation via cascaded attention decoding. In *Proceedings of the IEEE/CVF Winter Conference on Applications of Computer Vision*, pages 6222–6231, 2023.
- [34] Reza Azad, Moein Heidari, Moein Shariatnia, Ehsan Khodapanah Aghdam, Sanaz Karimijafarbigloo, Ehsan Adeli, and Dorit Merhof. Transdeeplab: Convolution-free transformer-based deeplab v3+ for medical image segmentation. In *International Workshop on PRedictive Intelligence In MEdicine*, pages 91–102. Springer, 2022.
- [35] Chenyu You, Ruihan Zhao, Fenglin Liu, Siyuan Dong, Sandeep Chinchali, Ufuk Topcu, Lawrence Staib, and James Duncan. Class-aware adversarial transformers for medical image segmentation. *Advances in Neural Information Processing Systems*, 35:29582–29596, 2022.
- [36] Ilya Loshchilov and Frank Hutter. Decoupled weight decay regularization. *arXiv preprint arXiv:1711.05101*, 2017.
- [37] Xizhou Zhu, Weijie Su, Lewei Lu, Bin Li, Xiaogang Wang, and Jifeng Dai. Deformable detr: Deformable transformers for end-to-end object detection. In *International Conference on Learning Representations*, 2020.
- [38] Zhengzhong Tu, Hossein Talebi, Han Zhang, Feng Yang, Peyman Milanfar, Alan Bovik, and Yinxiao Li. Maxvit: Multi-axis vision transformer. In *European conference on computer vision*, pages 459–479. Springer, 2022.